



Observation of Ice Pellets and its Association with Meteorological Conditions in the Yeongdong Region of Korea

Yu-Jin Chae^{1,4} · Byung-Gon Kim¹ · Young-Gil Choi^{1,2} · Ji-Hoon Jung^{1,3} · Ji-Yun Kim¹ · Byung-Hwan Lim² · Ki-Ho Chang⁴

Received: 26 September 2023 / Revised: 3 March 2024 / Accepted: 12 March 2024
© The Author(s) 2024

Abstract

The microphysical properties of ice pellets (IP) are analyzed, and associated relevant thermodynamic conditions are investigated using rawinsonde soundings and model reanalysis data in the Yeongdong region of Korea. During the intensive observation campaign of snowfall, two distinctive IP events of 1 March 2021 (IP1) and 15 March 2018 (IP2) were observed when strong cold advection was prevalent below about 2 km as accompanied by distinctive inversion strength (4.7–9.3 °C) above the cold layers. Cold air intrusion along the eastern side of Taebaek mountains appeared to abruptly decrease low level (850 hPa) temperature up to -4.7 ~ -3.4 °C, but warmer than 8-year average (-9.5 °C), respectively. Both episodes had smaller maximum size (1.8 mm in average) of ice pellets with greater fallspeed (4.2 m s⁻¹) in comparison to general snow crystals. Ice pellets occurred in the synoptic condition of the High in the north and the Low passing by the south, which resulted in cold northeasterly over the Yeongdong region. Rawinsonde soundings show a melting layer between 800 and 700 hPa just above the freezing layer of 900 ~ 800 hPa existed, such as a reversed S temperature profile, which is also consistent with the model reanalysis. The IPs' life time was short within a couple of hours since it occurred along with low-level strong cold advection (IP1) or rapidly-moving squall line (IP2).

Keywords Yeongdong · Rawinsonde · Cold air · Ice pellet · Fallspeed

1 Introduction

Solid precipitation in winter is hard to measure because of various ice particle habits and shapes, depending on temperature and humidity. Particularly, ice pellet (IP) of all snow crystal habits is a small and translucent ice with its diameter less than 5 mm, and freezing rain (FR) is also known to be frequently accompanied with IP (Gibson and Stewart 2007;

Bourgouin 2000). Supercooled droplets freeze into freezing rain when they contact with the ground below the freezing temperature, whereas ice pellets form when they freeze in the middle of subfreezing layer (Rauber et al. 2000; Stewart and Crawford 1995). Both types can be regarded as freezing precipitation (FP) in winter. Especially freezing precipitation is a hazardous wintertime weather phenomenon, specifically in Canada, United States, and East Asia (Bernstein 2000; Rauber et al. 2001; Cortinas et al. 2004; Matsushita and Nishio 2008; Gao et al. 2013; Deng et al. 2015), resulting in substantial number of injuries and fatalities, along with severe traffic accidents including aircraft icing issues (Bernstein and Omeron 1998; Bernstein 2000). Specifically, Houston and Changnon (2007) showed that FR has even more severe societal impact than snowfall or rainfall for the same mass of precipitation. Therefore, Ralph et al. (2005) emphasized the importance of understanding the habit and shape of solid precipitation to predict the possible hazardous weather.

Roberts and Stewart (2008) identified various kinds of synoptic and surface conditions when IP occurred in the arctic region using the rawinsonde soundings and model

Responsible Editor: Byung-Gon Kim

✉ Byung-Gon Kim
bgk@gwnu.ac.kr

¹ Department of Atmospheric Environmental Sciences, Gangneung-Wonju National University, 7 Jukheongil, Gangneung 25457, Gangwon, Korea

² Forecast Research Department, National Institute of Meteorological Sciences, Seogwipo, South Korea

³ National Meteorological Satellite Center Korean Meteorological Administration, Seoul, South Korea

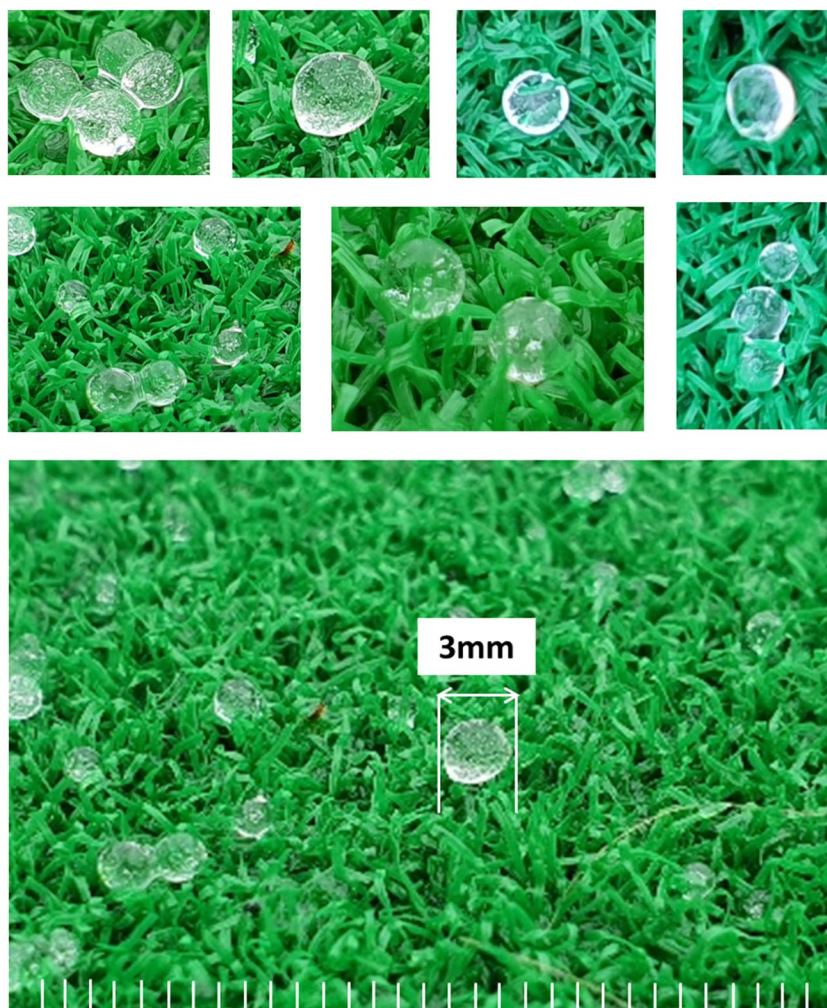
⁴ Research Application Department, National Institute of Meteorological Sciences, Seogwipo, South Korea

reanalysis data. Kochtubajda et al. (2017) conducted a climatological analysis of FR and IP in the northern Canada, and discussed their association with Chinook. In addition, Nagumo and Fujiyoshi (2015, 2017) examined the micro-physical characteristics of IP along with abnormal warm and dry air intrusion in the relevant storm, and explained the refreezing processes of melting snowflakes by evaporative cooling. While there have been many FP studies all over the world, no FP event has been quantitatively investigated in Korea until now. A couple of IP events were observed during the period of an intensive snowfall observation campaign when atmospheric thermodynamic profiles and multiple pictures of snow crystals were obtained. One was observed during the transition of rain to snow along with an abrupt drop in temperature on 15 March 2018, and the other was 1 March 2021 when IPs were observed for the very short period within an hour in the transition period of rain to snow. In general, most IP events are short lived (<2 h) (Cortinas et al. 2004) although IP lasted for 10 h in northern Japan on 10 April 2005 (Nagumo and Fujiyoshi 2015).

The events of 1 March 2021 and 15 March 2018 are named as IP1, and IP2, respectively. The pictures of ice pellets during IP1 are obtained with a smartphone camera as well as MASC (Multi-Angle Snowflake Camera). Overall ice pellet particles taken by a smartphone were very clear and transparent with its size less than 3 mm as shown in Fig. 1. Beside IP, the other dominant habit was in the form of aggregates which were very sticky and heavy because of its surface melting.

In winter, the Yeongdong region of the Korean Peninsula has frequently heavy snowfall which is largely initiated by the East Sea effect, due to a larger difference between air and sea surface temperatures, and further enhanced by orographic effect (Nam et al. 2014; Lee et al. 2012). Cold northeasterly flow appears to accumulate in the eastern slope of the Taebaek mountains as the negative buoyance of colder air is much greater than the momentum specifically in winter (Kim et al. 2021a). In addition, this kind of cold air accumulation (or damming) eventually results in preventing the snow clouds formed over the East Sea from

Fig. 1 Photographs of ice pellet (IP) particles during the campaign (i.e. IP1) taken from 1230 to 1300 KST on 1 March 2021 using a smartphone. The interval between white lines is equivalent to 1 mm



penetrating inland and sometimes makes it hard to forecast snowfall in the Yeongdong region (Kim et al. 2021b). On the other hand, cold air intrusion in the lower layer could lead to phase change of solid precipitation, such as FR and IP, along with the warmer air above the freezing layer, which also makes the wintertime forecast even harder in the region. Therefore, we need to understand the location, time, and phase of mixed precipitation for a more accurate estimation of wintertime precipitation. This study is the first to address the characteristics of IP and its relevant meteorological condition in Korea, and may be a solid foundation for future investigations of IP.

This paper is organized as follows. Section 2 briefly describes the observation and the analysis method. Section 3 first presents the general feature of snowfall in the Yeongdong region, and the microphysical properties of ice pellets (IP) as well as its association with meteorological conditions. In addition, vertical profiles and horizontal distributions of thermodynamic properties during the IP events are investigated using the model reanalysis data. Finally the conclusions are presented in Section 4.

2 Methodology

Gangneung (a primary observation site) is located just east of the Taebaek mountain range and also adjacent to the East Sea. The mountain range stretches from the northwest to the

southeast covering a length of approximately 600 km, with an average elevation from 800 to 1,000 m. The East Sea has a surface area of about 10^6 km² and an average depth of 1,800 m. Especially during late winter, a primary season for heavy snowfall, the sea surface temperature near Gangneung is relatively warm, ranging from 8 to 12 °C. This warmth plays a crucial role in East Sea effect snowfall (SES) in Yeongdong. The stations and the main analysis domain for the study are displayed in Fig. 2.

The observation campaign, Experiment on Snow Storms At Yeongdong (ESSAY), has been conducted in the Yeongdong region to intensively observe snowfall from February to March since 2014 to the present (Ko et al. 2016; Kim et al. 2018). Specifically, rawinsonde soundings were made at Gangneung whenever snowfall was forecasted in the Yeongdong region during the ESSAY campaign. The rawinsondes were launched every 6 h at 0000, 0600, 1200 and 1800 KST at Gangneung-Wonju National University (GWNU), and 0300, 0900, 1500, and 2100 KST at Gangwon Regional Meteorological Office (GRMO), respectively. GRMO is located just 4 km from GWNU. Therefore 3-hourly vertical profiles of thermodynamic structure can be obtained at Gangneung for the Yeongdong region. The brief summary of observation is explained in Table 1. In addition, surface temperature, precipitation, and snowfall accumulation measured at a neighboring Automatic Synoptic Observing System (ASOS) of GRMO were also used for the analysis.

Fig. 2 The main analysis domain (Yeongdong enlarged) with the observation site (Gangneung) in Korea. GRMO indicates Gangwon Regional Meteorology Office (GRMO) and GWNU stands for Gangneung Wonju National University, both of which are located at Gangneung

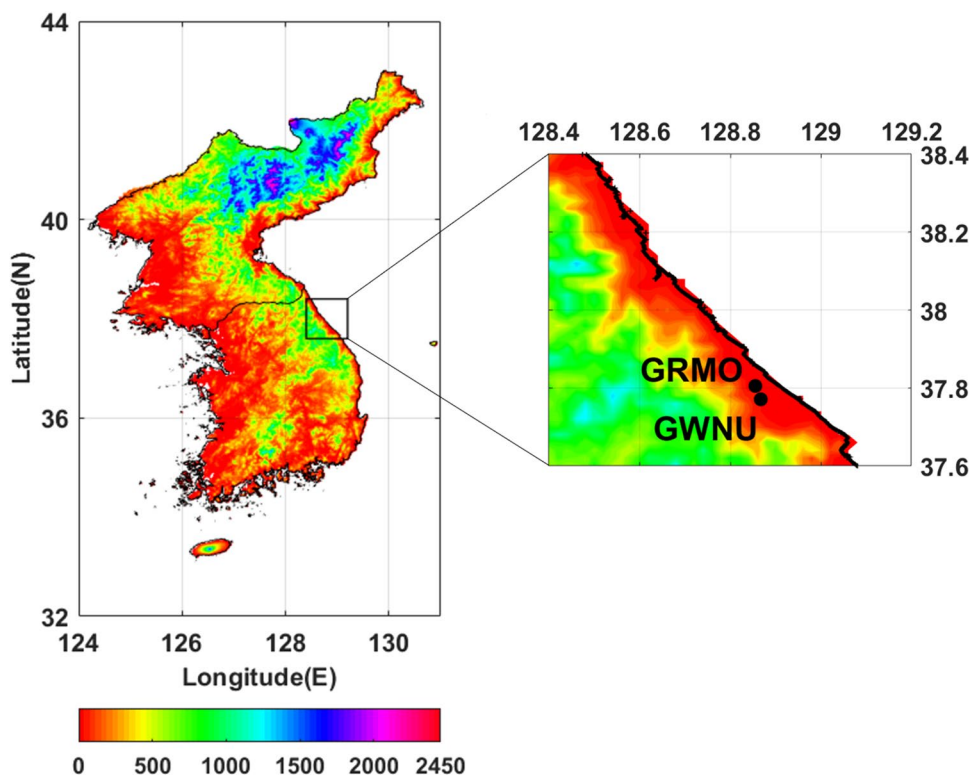


Table 1 An overview of main observational instruments and analysis stations used in this study

Instruments	Site	Lat (N°)	Lon (E°)	Manufacture/Model	Variable
Rawinsonde	GWNU	37.771	128.867	GRAW/DFM-09	Temperature, pressure, wind direction, wind speed, humidity, dew-point temperature
	GRMO	37.805	128.855	Vaisala/RS41-SG	
Rain gauge	GRMO	37.805	128.855	OTT/Pluvio2	Snowfall, precipitation
GNSS	GWNU	37.771	128.867	Trimble	Precipitable water vapor
MASC	GWNU	37.771	128.867	Fallgatter Tech/	D_{\max} , fallspeed, complexity, aspect ratio, orientation, riming index

GWNU Gangneung-Wonju National University

GRMO Gangwon Regional Meteorological Office

GNSS Global Navigation Satellite System

MASC Multi-angle snowflake camera

Table 2 Specifications of local data assimilation and prediction system (LDAPS) used in this study

Horizontal resolution	1.5 km 602 × 781
Vertical layers	Layer 70 (Top of Height ~40 km)
Prediction period	0000, 0600, 1200, 1800 KST 0300, 0900, 1500, 2100 KST
Variables	U-component of wind V-component of wind Temperature

KST Korean standard (local) time

However, the ESSAY campaign has limitations on spatial distribution of thermodynamic characteristics since it mainly consists of frequent vertical soundings at both neighboring sites. Thus, horizontal and vertical distributions of temperature and wind fields were examined using Local Data Assimilation and Prediction System (LDAPS) reanalysis, which is produced every 3 h in the horizontal resolution of 1.5 km and 70 vertical layers based on the Unified Model by Korean Meteorological Administration (Shin et al. 2022). Detailed information of LDAPS used in this study is summarized in Table 2.

Multi-Angle Snowflake Camera (MASC) has been used for the quantitative analysis of snowflakes since 2017. MASC measures multi-angle high-resolution images and fall speed of hydrometeors during free fall (Garrett et al. 2012). Fall speed is calculated from the time it takes for an ice particle to traverse the distance between the upper and lower triggering array. The pictures of falling hydrometeors are used for the classification of their habits and phase (Praz et al. 2017) in order to identify ice pellet occurrence. Precipitation in winter consists of rain, freezing rain, ice pellet, graupel, and snow flake, etc. In general, precipitation type and phase depend on temperature profiles along with the height of freezing level and thickness of the subfreezing layer (Carmichael et al. 2011). Of all types of solid precipitation, ice pellet can be formed when an ice particle falls through the melting layer above 0 °C and refreezing layer

below, which make it possible for the ice to melt partly or completely and further refreeze into IP below the melting layer (Hanesiak and Stewart 1995). In this study, the vertical profile of wet-bulb temperature for the IP occurrence is called as ‘a Reversed S profile’, as demonstrated in Fig. 3. In addition, a flow chart to classify ice pellet is also represented using mainly surface T_w , maximum and minimum of T_w , as well as vertical profile of T_w , adapted from Schuur et al. (2012). That is, if surface T_w is greater than 0 °C and less than 3 °C, T_w of mid-level melting layer is greater than 0 °C and less than 2 °C, and finally T_w of low-level refreezing layer is less than -5 °C, then IP can be observed at the surface. This kind of criteria is useful to check IP occurrence since time scale of IP is quite short within a couple of hours. Unfortunately, as the observation campaign was not intended for the IP analysis, the multi parameter radar analysis was not available for the further understanding of the IP characteristics.

3 Results

3.1 General Features

The Yeongdong region has frequent heavy snowfall episodes when cold air outbreaks occur over the warmer East Sea specifically in late winter (Lee et al. 2012), which is named as ‘East Sea effect Snowfall (SES)’ (Nam et al. 2014), basically similar to lake effect snowfall well known in the world. This kind of heavy snowfall (SES) tends to be frequently accompanied with a strong inversion since cold northeasterly flow penetrates below relatively warmer layer along with dominant upper westerly flow. Therefore, snow clouds formed in the convective unstable condition over East Sea appear to be stratiform largely capped by strong inversion (Kim et al. 2018, 2021a). The number of snowfall events observed in the campaign (2014 – 2021) is 51, of which SES only is 28. The other events are associated with synoptic driven snowfall or other extreme events such as tropopause folding, which will not be discussed in this study.

Main meteorological characteristics for the 28 SES events are summarized in Table 3. General characteristics of SES indicate that mean 850 hPa temperature is $-9.5\text{ }^{\circ}\text{C}$

with its cloud top height of 2.3 km and precipitable water vapor of 8.5 mm. In addition, a strong inversion frequently exists with its mean strength of $2.4\text{ }^{\circ}\text{C}$ and depth of 440 m.

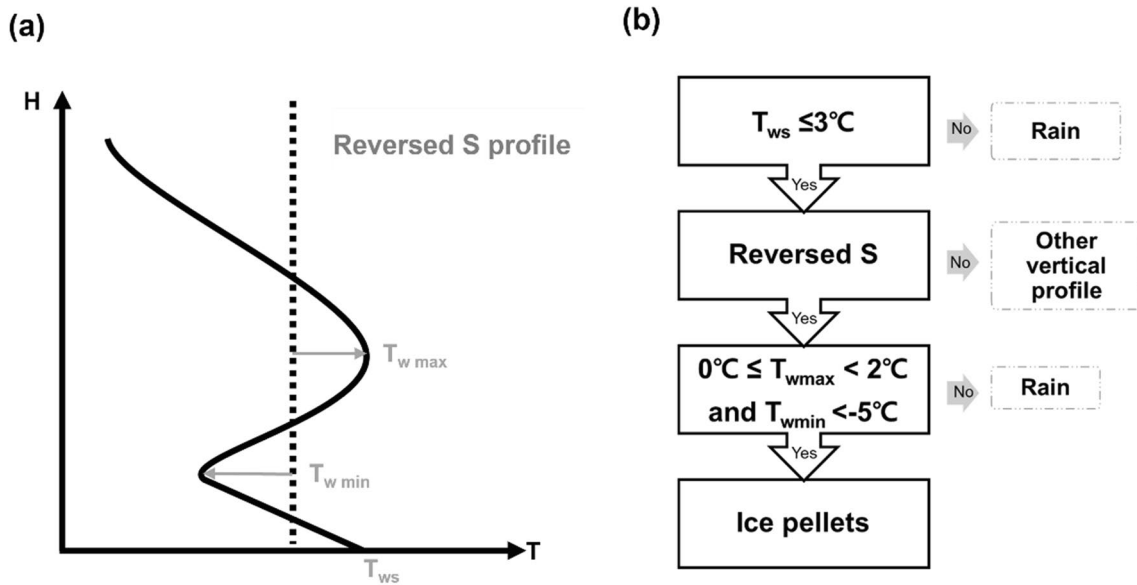


Fig. 3 Wet-bulb temperature profile for the IP occurrence (a) and a brief IP classification flowchart (b) based on Schuur et al. (2012). A reversed S profile is indicative of bilateral symmetry of S profile. T_{ws}

is surface wet-bulb temperature, and T_{wmax} and T_{wmin} are maximum and minimum of T_w , respectively

Table 3 Mean and standard deviation of cloud top height, 850 hPa temperature, inversion and precipitable water vapor (PWV) for the ESSAY and IP events

Day	CTH (km)	T_{850} ($^{\circ}\text{C}$)	Inversion		PWV (mm)
			Thickness (m)	Strength ($^{\circ}\text{C}$)	
ESSAY	2.3 ± 0.6	-9.5 ± 3.7	443.1 ± 243	2.4 ± 1.4	8.5 ± 2.8
IP events					
2021.03.01	NA	-3.4	564	4.7	21.1
2018.03.15	3.1	-4.7	292	9.3	18.7

ESSAY Experiment on snow storms at Yeongdong; IP Ice pellet; CTH Cloud top height; T_{850} 850 hPa temperature; PWV Precipitable water vapor; SD Standard deviation; NA Not available

Fig. 4 Vertical profiles of temperature (yellow) and dew-point temperature (cyan) for total of 154 rawinsonde soundings for the SES events only. Thick red and blue lines indicate those of temperature (solid) and dew-point temperature (dashed) on 01 March 2021 (IP1) and 15 March 2018 (IP2), respectively

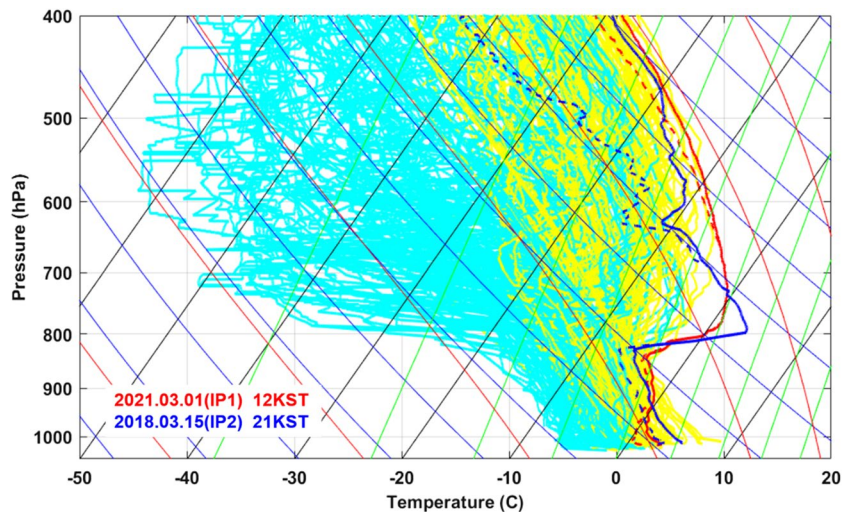


Figure 4 shows vertical profiles of the dry bulb (yellow) and dew point (blue) temperatures obtained from 154 rawinsonde soundings for SES events, which represents the moist cloud layers below around 800 hPa (~ 2 km) where both temperatures are close to each other, indicative of higher relative humidity. A distinctive dry layer above the clouds exists, which is also consistent with the cloud top height as in Table 3. Cloud top height is determined using temperature and dew point temperature difference from rawinsonde soundings.

3.2 Ice Pellet Analysis

Figure 4 displays vertical profiles of temperature and dew-point temperature for ice pellet episodes (IP1 and IP2) as overlapped with 154 snowfall events, when IP was observed around 1200 KST 1 March 2021 and 2100 KST 15 March 2018, respectively. Both events have the remarkable inversion strength, such as 4.7°C for IP1 and 9.3°C for IP2, which are much greater than the SES average (2.4°C). As a result, IP tends to occur when much warmer atmosphere in the mid-layer exists with 850 hPa temperature of -3.4°C and -4.7°C for both IP events as demonstrated in Fig. 4. Mid-level warm layer above the freezing temperature provide ice particles enough time to partially or fully melt. Later, melting particles freeze again during the passage through subzero layer with more than 1 km thickness. This kind of thermodynamic profile was also accompanied with much higher precipitable water vapor (19–21 mm) and the warmer temperature ($-4.7\sim-3.4^\circ\text{C}$) than the averages (8.5 mm and -9.5°C , respectively). It is interesting to note that both IP events had very humid condition within a couple of hours.

For the quantitative analysis of IP, frozen and partially melted hydrometeors are examined using a MASC. Figure 5 shows the images of ice pellets during IP1 and IP2 events. The period of IP captured is from about 1230 to 1300 KST during the IP1 event (1 March 2021), while that

is from 2130 to 2330 KST during IP2 (15 March 2018). Both events indicate a short time scale of IP such as less than a couple of hours only. In general, the images of water droplets and melting ice particles are dark and black since they tend to absorb light of three illuminating diodes. If a melting particle is reflected in a half round form with its original brightness dimming, its maximum dimension calculated appears to be smaller than its actual size, which is an inherent measurement artifact of MASC. Maximum sizes of both IP1 and IP2 increased from 0.9 and 1.0 mm to 1.9 and 1.6 mm, respectively, after being modified and recalibrated from the melting particle image by considering the underestimation of its size.

Figure 6 indicates the relationship of the fallspeed to the maximum dimension of solid precipitation. Blue line is an empirical formula of raindrops (Atlas and Ulbrich 1977) while the black line is that of rimed aggregates (Ishizaka 1995; Ishizaka et al. 2013). Through the careful and visual check of ice particles, erroneous data (25%) of unusually lower fall speed (close to 0) were manually discarded, which mostly resulted from the mismatches in detected particles when two particles pass through the measurement slot almost at the same time as previously mentioned in Nagumo and Fujiyoshi (2015). The dots appear to exist between blue and black lines in spite of very scattered distribution (Fig. 6). The relationship of fallspeed of ice pellets against their dimension shows largely similar characteristics of rain droplet, but partly some of rimed snow without any distinct mode. IP particles captured in the camera were very few (only 60), and thus detailed microphysical analysis of IP was very limited. Nagumo and Fujiyoshi (2015) reported both fast falling (rain droplet) and slow falling (light hailstone) modes of long-lasting (10 h) ice pellets formed by freezing associated with evaporative cooling due to an unusually warm and dry atmosphere in northern Japan.

The analysis results are summarized in Table 4. The average fallspeed and maximum dimension of IP events are

Fig. 5 Images of ice pellets taken by MASC on (a) 01 March 2021 (IP1) and (b) 15 March 2018 (IP2). The brightness and contrast of IP images are manually enhanced for the further analysis

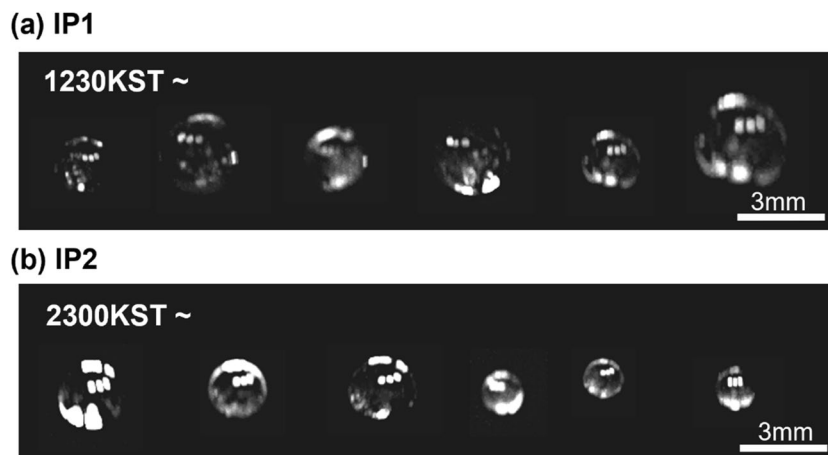


Fig. 6 Scatter plot of fallspeed vs. D_{max} for IP1 (red dot) and IP2 (blue dot) events. The blue and black solid lines are the empirical formula of rain and densely rimed aggregates (Atlas and Ulbrich 1977; Ishizaka 1995)

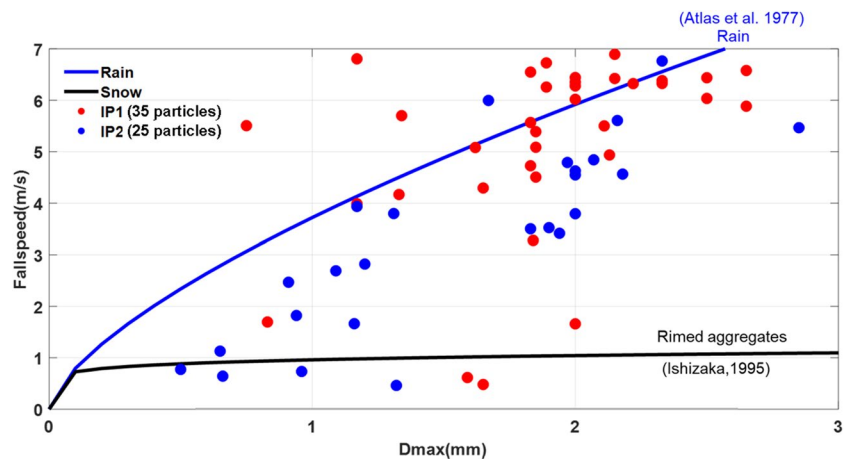


Table 4 Mean and standard deviation of fallspeed and D_{max} for IP event as compared with 9 SES events for the ESSAY campaign

Episode	Date	Period (KST)	Fallspeed (m/s)	D_{max} (mm)
			Mean \pm std	Mean \pm std
IP	2018.03.15	2100~2300	3.3 \pm 2.1	1.6 \pm 0.6
	2021.03.01	1200~1300	5.1 \pm 2.5	1.9 \pm 0.4
Mean			4.2 \pm 2.3	1.8 \pm 0.5
SES	2017.01.20	1100~1800	1.1 \pm 0.8	3.0 \pm 2.4
	2018.01.22~23	1700~0400	1.0 \pm 0.5	3.6 \pm 2.6
	2018.02.24~25	1500~0900	NA	1.1 \pm 0.3
	2018.03.08~09	0000~1200	1.5 \pm 0.6	3.5 \pm 2.0
	2019.01.31	1300~2000	1.0 \pm 0.8	2.3 \pm 1.7
	2020.02.08	2000~2300	1.2 \pm 1.0	3.1 \pm 2.7
	2021.03.01	1300~2300	1.3 \pm 0.9	3.3 \pm 2.4
	2021.03.06	0300~2300	1.8 \pm 1.1	1.3 \pm 0.4
	2021.12.24~25	1900~0900	1.3 \pm 0.9	3.3 \pm 3.0
Mean			1.3 \pm 0.8	2.7 \pm 1.9

IP Ice pellet

SES East sea effect snowfall

ESSAY Experiment on severe snowfall at Yeongdong

4.2 m s⁻¹, and 1.8 mm, respectively, whereas those for nine SES events are 1.3 m s⁻¹, and 2.7 mm. Therefore, the sizes of IPs are smaller with much faster fallspeed than those of typical SES snowflakes.

3.3 Meteorological Condition

Figure 7 shows synoptic charts of 850 hPa and 700 hPa for both IP episodes. First, there are accumulated snowfall amounts of 43.3 cm for 2 days (1–2 March 2021) during the IP1 period. On 1 March, precipitation began early morning with warm and moist southwesterly as the low-pressure system approaching. Ice pellets were captured at the strong

snowfall intensity of 2.6 cm hr⁻¹ (precipitation intensity of 6.4 mm hr⁻¹) mainly around noon along with cold northerly/northeasterly when the low was located at the center of the Korean peninsula. Surface temperature decreased by 6 °C from 0600 to 1500 KST even during the day time. Meanwhile, warm advection (southwesterly) above 2 km (ex. 800 hPa) occurred in the Yeongdong region with the upper trough over the Yellow Sea.

The next event (IP2) was observed at midnight on 15 March 2018 when surface temperature abruptly dropped from 20.8 °C (noon) to 2.4 °C (midnight) for 10 h. Precipitation started as rain shower around 1800 KST as a squall line passed by and gradually changed to ice phase late night. This kind of abrupt decrease in temperature was also shown in the IP1 episode. As shown in Fig. 7, the warm advection from the southwest aided by a weak Foehn caused an increase in temperature up to 20.8 °C during the daytime in the Yeongdong region. Both IP1 and IP2 events were observed in March, the change of seasons from winter to spring, when weather system tends to abruptly change. The High system to the north and the Low passing by the south are frequently set up as Siberia High is liable to expand to the east in late winter. After all, the cold northeasterly with blocking of the Taebaek mountain range can facilitate low-level rapid cooling, which underscores strong cold advection and stronger inversion along with the warmer layer above.

Figure 8 demonstrates vertical soundings of temperature and wind obtained from rawinsondes for the IP1 period. A reversed S profile is well represented from 0900 to 1400 KST, a sort of bilateral symmetry of S alphabet. During the period, low-level cold advection occurred when northerly and northeasterly was exhibited from 900 hPa (0900 KST) up to 800 hPa level (1400 KST) whereas warm southwesterly was consistent above the cold layer. Note that the launched balloon at noon reached only 1.5 km and returned to the ground since lots of sticky snow crystals adhered to the surface of the balloon. The additional sounding at 1400

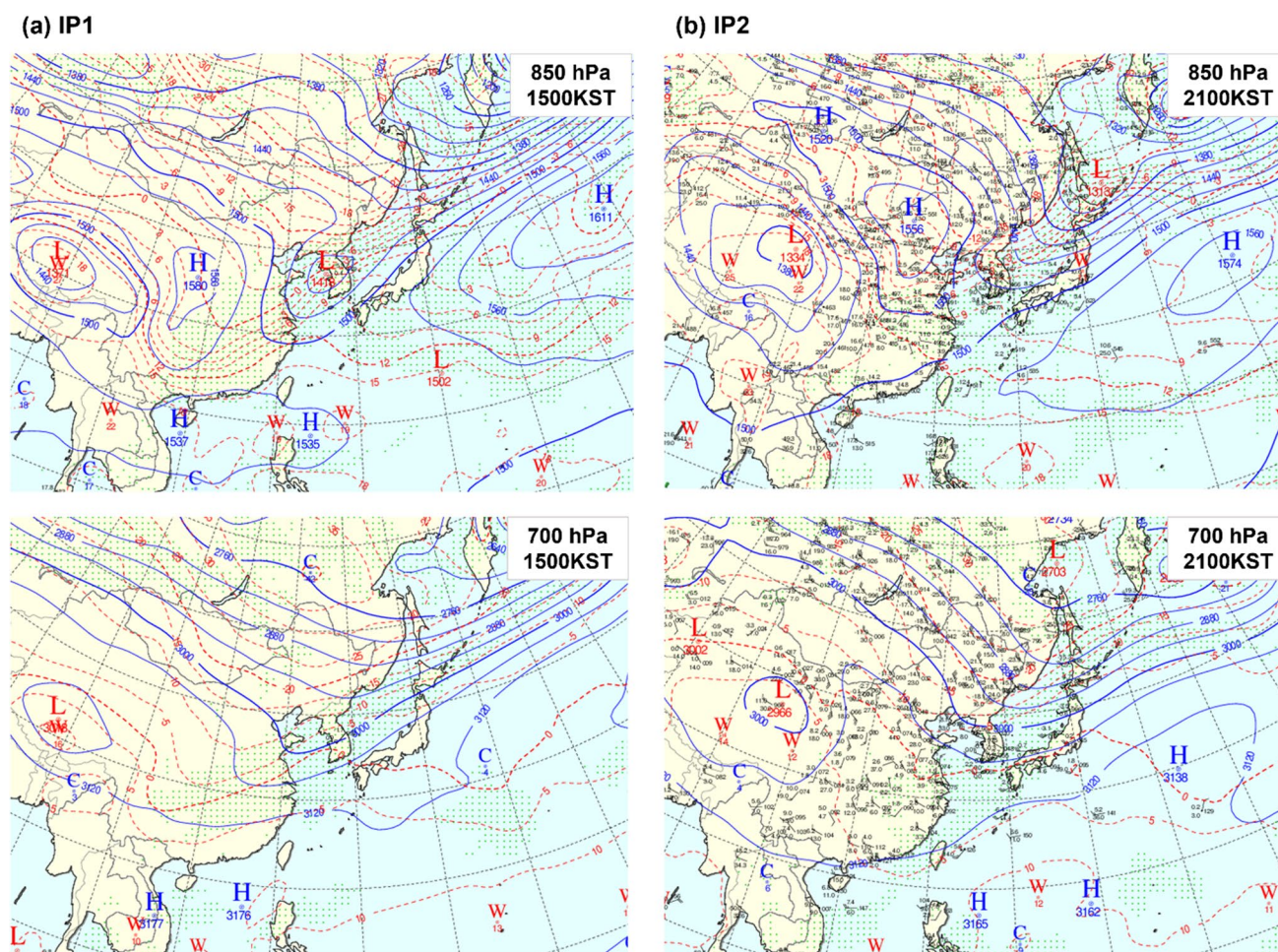


Fig. 7 Synoptic charts of 850 hPa and 700 hPa of (a) 01 March 2021 (IP1) and (b) 15 March 2018 (IP2). Blue line and red dashed line indicate geopotential height and temperature, respectively. Green dots denote humid region

KST was done for 1200 KST. Therefore, the missing profile of 1200 KST was interpolated by using 0900 and 1400 KST profiles as displayed in blue line in Fig. 8. The interpolated profile shows a melting layer from 800 to 750 hPa and the deeper refreezing layer below 800 hPa level. Right panel of wind profile further supports northerly flows below 2 km, and southerly and southwesterly above 2 km. Lower panel of Fig. 8 exhibits temporal variations of 3 hourly snowfall amount, snow water equivalent, and surface temperature. While surface temperature decreased from 6 °C (0600 KST) to 0 °C (1500 KST) even during the day, IP particles were captured by both MASC and smart phone around noon during the rapid cooling process.

Figure 9 displays rawinsonde soundings for the IP2 period from 1500 to 2400 KST on 15 March 2018. Interestingly, the dominant westerly existed in the whole layer at 1500 KST but low-level wind abruptly changed to northeasterly below 900 hPa at 1800 KST, and later deepened up to 850 hPa. Accordingly, the melting layer of 810 to 730 hPa

and refreezing layer of 940 to 810 hPa existed, which profile is consistent with that (a reversed S profile) of 1200 KST of IP1 event except for low-level rapid cooling with surface temperature drop of 19.3 °C (1500 KST) to 5.8 °C (1800 KST) as a squall line passing by. The precipitation phase was rain at first and changed to ice pellet at midnight by surface temperature approaching the freezing point. No snowfall accumulation was officially reported at nearby ASOS station (GRMO) though ice pellet was captured by MASC at GWNU.

Additionally, we estimated the period of ice pellet occurrence based on the solid precipitation classification method developed by Schuur et al. (2012), as shown in Fig. 10. Wet-bulb temperature was interpolated at 10 min interval from 0820 to 1420 KST for the IP1 event and 2040 to 2340 KST for the IP2 event. As a result, the period of ice pellet occurrence was estimated to be from 1240 to 1300 KST during the IP1 event, which aligns with the MASC image analysis. The positive area above the freezing temperature was minimal and significantly smaller than the negative area (below 0 °C), as

Fig. 8 Vertical profiles of temperature, dew-point temperature and wind ($m s^{-1}$) for 0900 and 1400KST 01 March 2021 (IP1). Interpolated sounding using 09 and 14KST is presented in blue. Black, blue, red, and green lines on background indicate isothermal, dry adiabat, wet adiabat, and saturation mixing ratio lines, respectively, in the thermodynamic diagram. Bottom figure denotes time series of accumulated snow depth (cm) and snow water equivalent (mm) amounts along with surface temperature

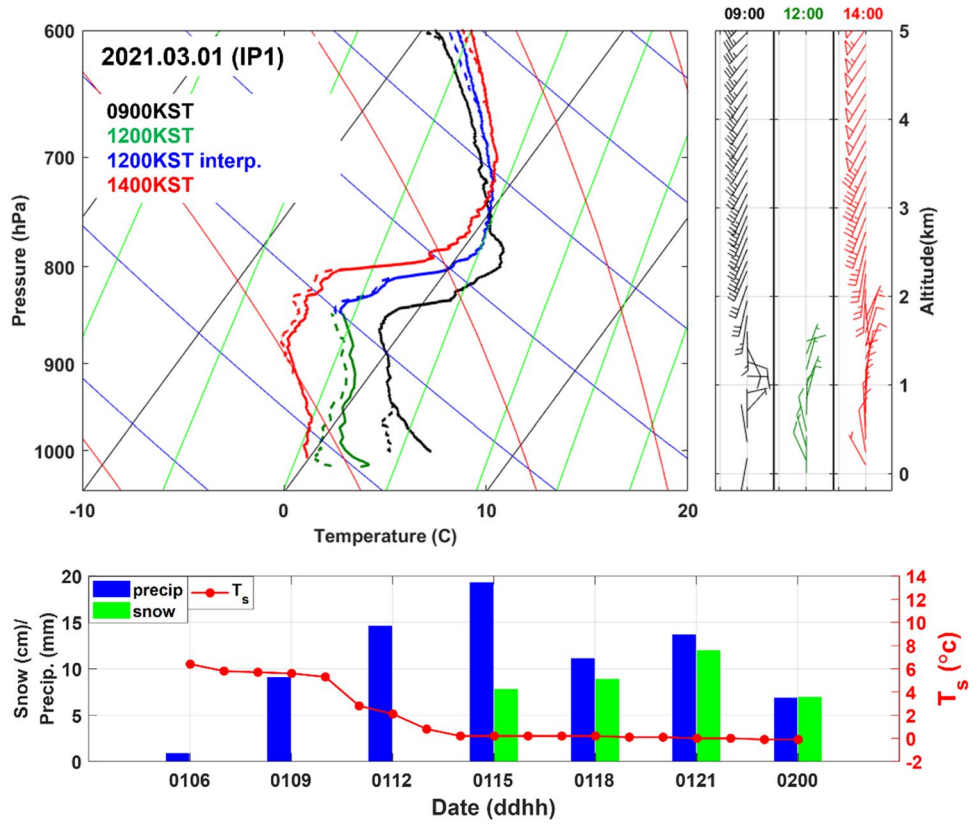


Fig. 9 The same as in Fig. 8 except for 15 March 2018 (IP2)

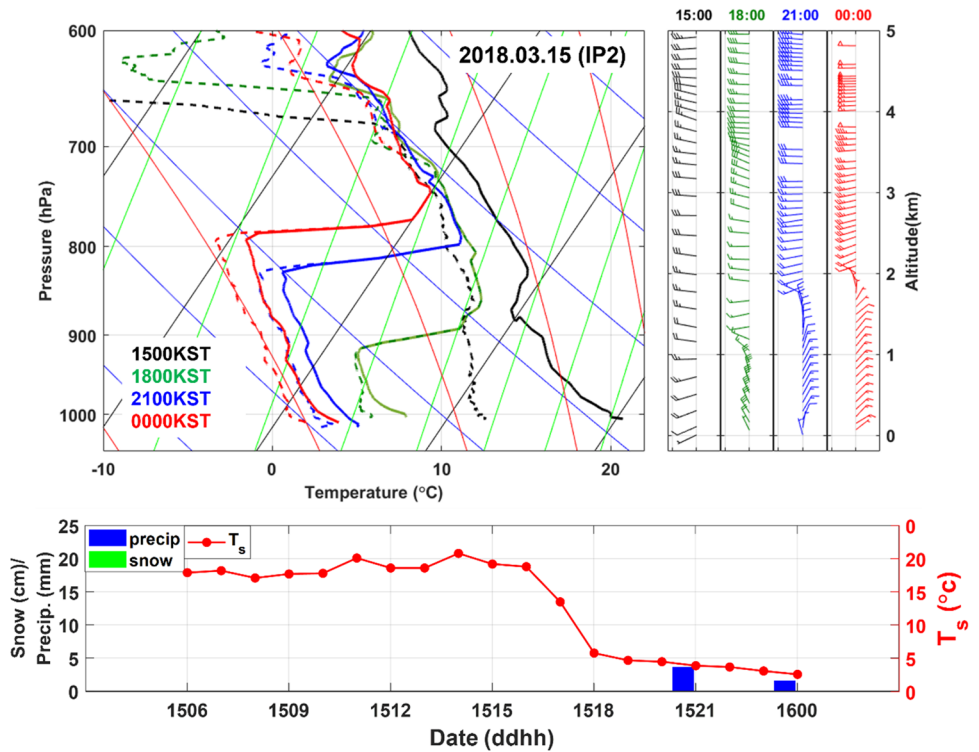


Fig. 10 Wet-bulb temperature profiles interpolated every 10 min interval (a) from 0820 to 1420 KST on 01 March 2021 (IP1) and (b) from 2040 to 2340 KST 15 March 2018 (IP2). The wet-bulb temperature ranges ($0^{\circ}\text{C} \leq T_{wmax} < 2^{\circ}\text{C}$ and $T_{wmin} < -5^{\circ}\text{C}$) are drawn in black dashed lines, respectively. The profile of blue lines belongs to the period (1240~1300 KST and 2130~2340 KST for the IP1 and IP2 events, respectively) when ice pellet could occur by Schuur et al. (2012) classification

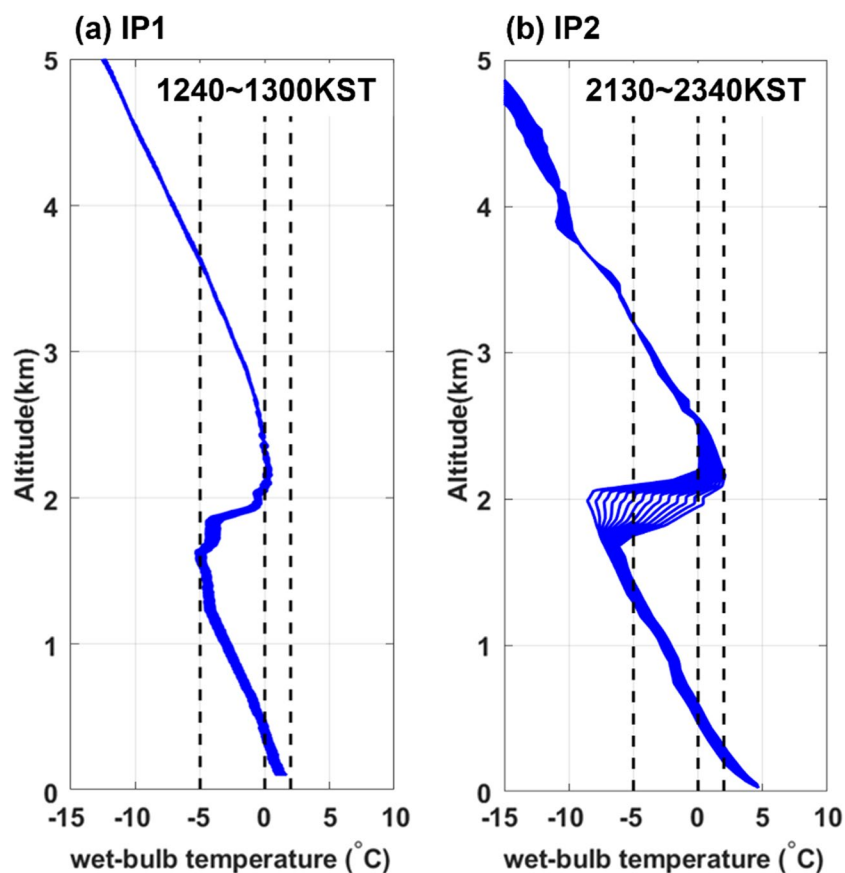
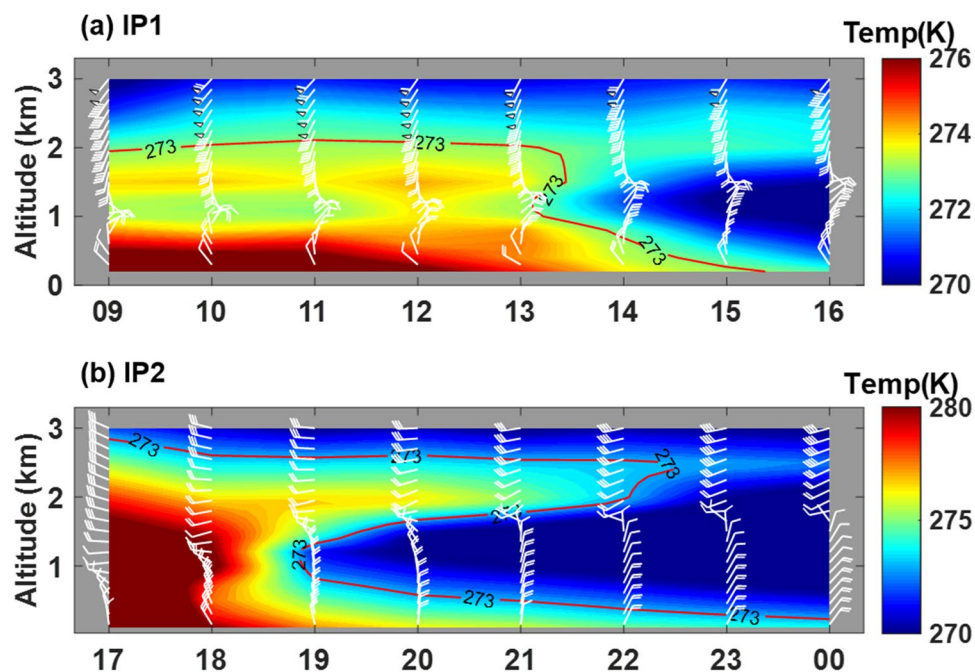


Fig. 11 Time series of vertical cross section of temperature and wind at GWNU for (a) IP1 (1 March 2021) and (b) IP2 (15 March 2018). The white flags are the horizontal wind, while the color shading denotes temperature with the red line 273 K (freezing temperature)



easily discerned. The duration of ice pellet occurrence during the IP2 event, meeting the classification criteria, was much longer (approximately 2 h), spanning from 2130 to 2340 KST, as the reversed S structure of T_w persisted for a longer period with more rapid cooling compared to the IP1 event.

3.4 Model Reanalysis

In order to overcome the spatial limitation of single-point sounding analysis, we examined temporal and spatial distributions of thermodynamic variables for the IP periods using LDAPS (Local Data Assimilation and Prediction System) from UM (Unified Model). Figure 11 exhibits temporal variations of vertical profiles of temperature and wind for the IP events. For the IP1 period (Fig. 11a), the northeasterly layer extended to 1 ~ 1.5 km while a warm southwesterly was present above 3 km during the same period as shown in Fig. 8. The speed of cold advection, as represented in LDAPS, appeared to be slower than that observed in the sounding data (see Fig. 8). This is evident because the temperature at

the 1 km altitude dropped to freezing at 1300 KST. Consequently, snowfall actually began earlier than the nighttime snowfall forecasted.

Meanwhile, cold advection during the IP2 period was much stronger than IP1 (Fig. 11b), indicative of much longer duration of IP (Fig. 9) as northerly began below 1 km since 1700 KST and developed up to around 2 km at 2100 KST. As a result, a melting layer from 2 to 2.7 km and a refreezing layer below existed at 2100 KST, which was well represented with LDAPS reanalysis data. The temperature variation of LDAPS was better consistent with that of the observation during the IP2 period than IP1 (Fig. 9).

In addition, vertical cross-section of temperature and wind of IP1 and IP2 obtained from LDAPS is demonstrated in Figs. 12 and 13, respectively. The cross-section diagram is drawn as a reference point of GWNU from the west (128.3 E) to the east (129.3 E). A melting layer of 1.5 to 2 km above the refreezing layer is also identified over GWNU during the IP1 period (Fig. 12). Afterwards the area of melting layer gradually decreased and finally disappeared at 1400 KST while the refreezing area increased. As the melting layer

Fig. 12 Vertical cross-sections of temperature and wind over the Yeongdong region during IP1 (01 March 2021). The cross section is drawn as a reference of GWNU from the west to the east (128.3 E to 129.3 E). The color shading and vectors denote temperature (K) and horizontal wind, respectively. The red lines mean the freezing temperature of 273 K. GWNU indicates Gangneung-Wonju National University

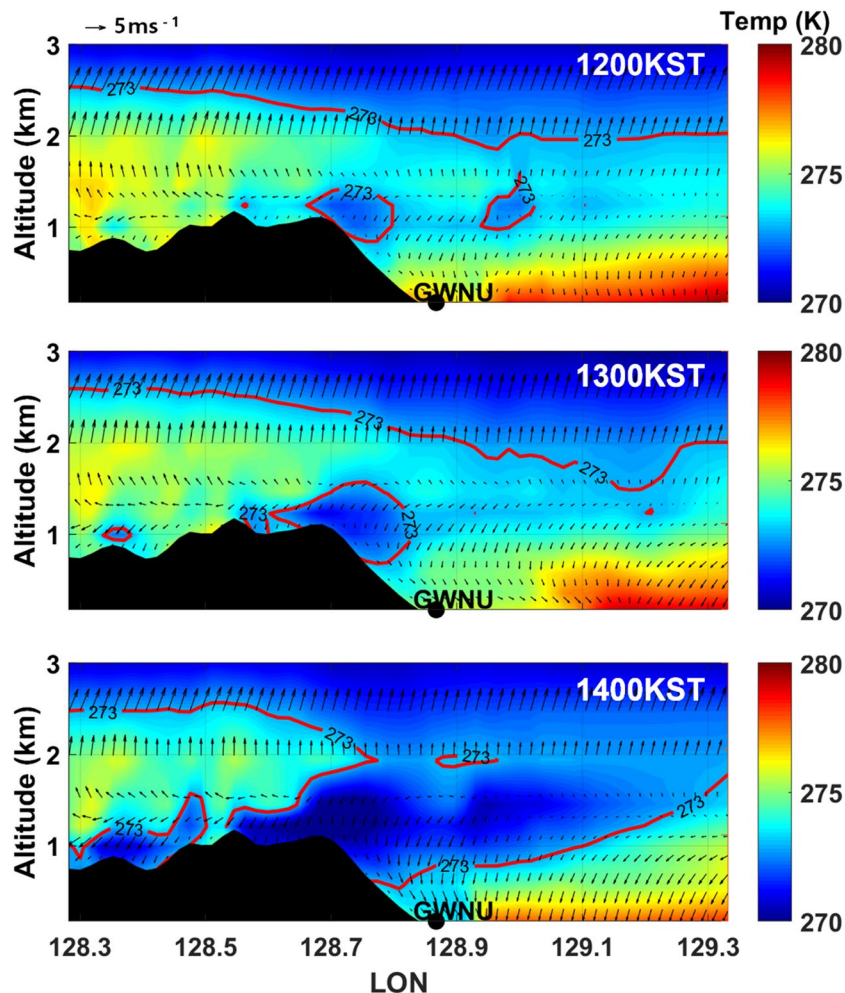
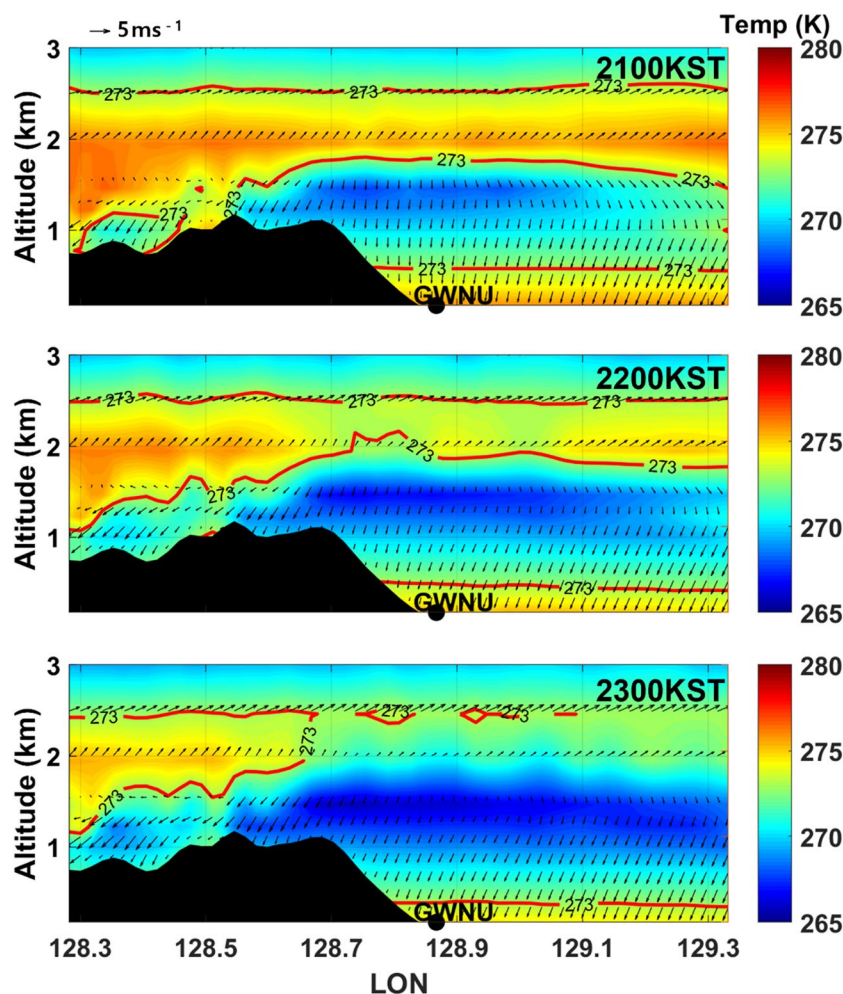


Fig. 13 The same as in Fig. 12 except for 15 March 2018 (IP2)



disappeared with a decrease in temperature, aggregates of snow crystals were observed on the ground. As mentioned in the previous section, ice pellet lifetime of the IP2 period was around 2 h (Fig. 13), longer than that (half an hour) of IP1. The longer duration of IP2 is thought to be associated with much stronger inversion strength such as 2 times greater than IP1 for a significant temperature drop in the lower level below the melting layer. Similar to IP1, the melting layer of IP2 from 2 to 2.5 km at 2100 KST gradually reduced and finally disappeared at 2300 KST while the refreezing layer was deepened with rapid cooling below 2 km as well represented in Fig. 13.

Figure 14 shows temperature and wind distributions of 900 hPa for both IP events. The 900 hPa level is selected as a middle level of cold air intrusion. In general, remarkable horizontal gradient of temperature was demonstrated from the northeast to the southwest along with cold air penetrating southward by time. The isothermal of 273 K for the IP1 event moved southward and passed over GWNU after 1200 KST. The similar pattern was also exhibited in IP2 wind fields. It is interesting to note that cold air passage

was largely parallel to the Taebaek mountain range for both IP events. The northwesterly flow looked like a barrier jet except for its intensity since its wind speed was relatively weak within 5 m s^{-1} . Cold northeasterly with negative buoyancy could not cross over the mountains and changed to northwesterly, and further flowed along the mountains as explained in Kim et al. (2021b). As a result, this kind of northwesterly barrier wind might help to bring about the lower level rapid cooling and IP occurrence in the Yeongdong region.

4 Discussion and Summary

In winter, cold air intrusion in the lower layer could lead to phase change of solid precipitation, which further makes the wintertime weather forecast even harder in the Yeongdong region of Korea. Therefore, we examined the general characteristics of two ice pellet events (15 March 2018 and 1 March 2021), and investigated the meteorological condition in association with IP occurrence for the purpose of

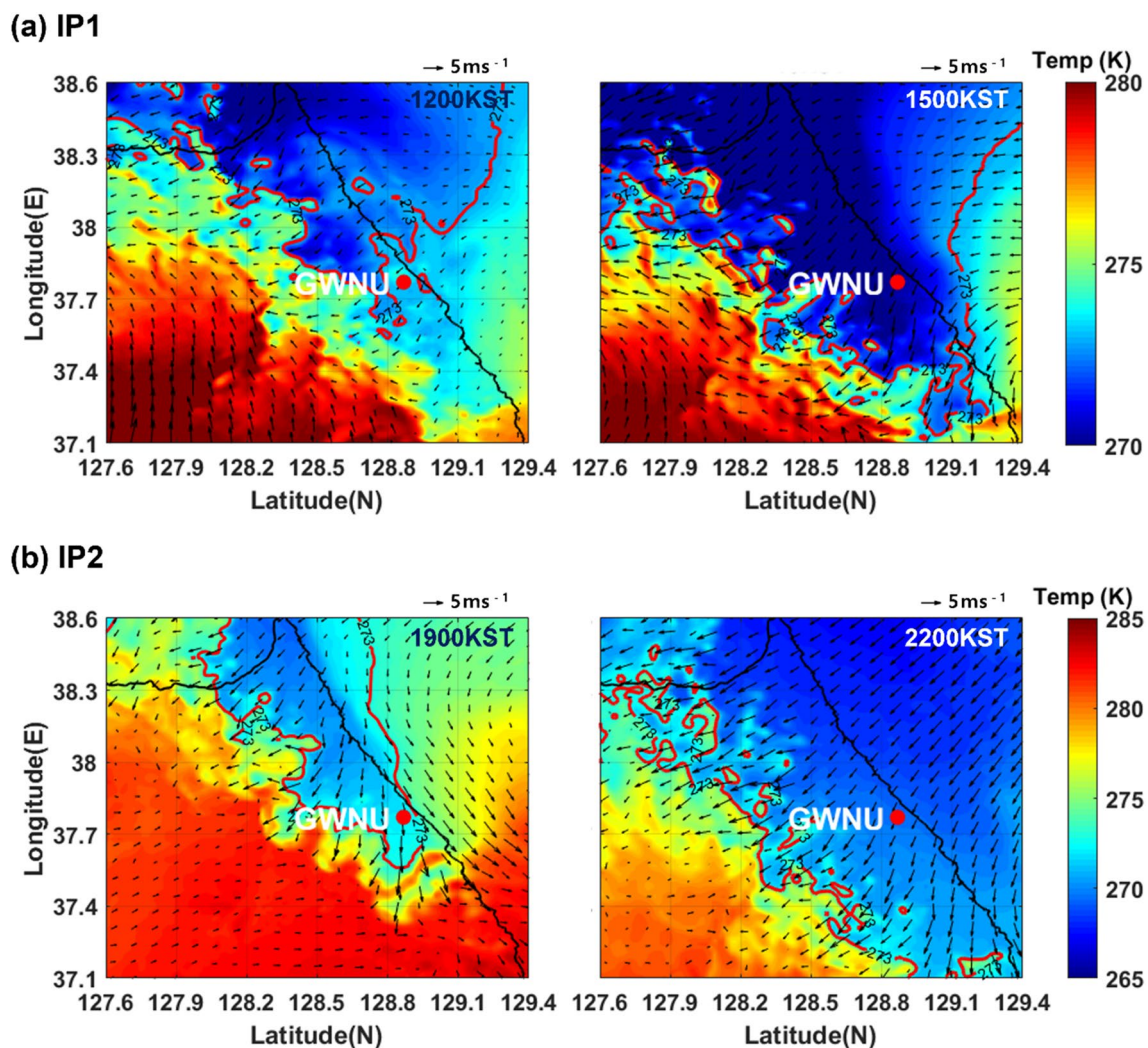


Fig. 14 Horizontal distribution of temperature (color shading) and wind field (vectors) on the 900 hPa level over the Yeongdong region for (a) IP1 (1 March 2021) and (b) IP2 (15 March 2018). Vectors denote horizontal wind and the red lines indicate 273 K

improving wintertime snowfall forecast. First of all, the meteorological conditions of IP events were compared with those of 28 SES (East Sea Snowfall) events, which indicates that 850 hPa mean temperature of the IP period $-4.7 \sim -3.4$ °C was warmer than that (-9.5 °C) of SES events. Furthermore, the inversion strength of IP was also $4.7 \sim 9.3$ °C greater than SES average (2.4 °C), and mid-level melting layer existed above the freezing zone. Both IP events occurred in March, a transition period from winter to spring.

Analysis of IP particles indicates that the average of its maximum dimension was 1.6~1.9 mm after the darkened images of melting snow were calibrated and unusually lower fall speeds (close to zero) of IP particles were discarded. Relationship of IP fallspeed to the maximum dimension represents relatively faster fallspeed (4.2 m s^{-1}) in spite of its smaller size (1.8 mm). The relationship of fallspeed

of ice pellets against their dimension shows similar characteristics of rain droplet with partly some of rimed snow. These IP events have very humid condition with precipitable water vapor of 19~21 mm, which is quite different from an unusually warm and dry condition in Japan (Nagumo and Fujiyoshi 2015) in which both fast falling (rain droplet) and slow falling (light hailstone) modes were shown for the long-lasting (10 h) ice pellets formed by freezing associated with evaporative cooling.

The synoptic analysis and rawinsonde soundings demonstrate that low-level cold northwesterly/northeasterly flow was facilitated by the synoptic setting of the Siberia High in the north and the Low passing by the south. Cold advection was prevalent below around 1~2 km as accompanied with strong inversion above the cold layer. Specifically, cold air intrusion with barrier wind along the eastern side of Taebaek mountains helped to significantly decrease low level temperature. Therefore, the

ice pellets of mixed precipitation occurred with a reversed-S profile of temperature during the phase change of solid precipitation, which is also identified with relatively warmer temperature of the 2–3 km layer above the cold air layer in late winter or early spring. Both IP events had a mid-level melting layer of 800–700 hPa above the freezing layer of 900–800 hPa, whose duration time was estimated to be 0.5 to 2 h, as also consistent with the LDAPS reanalysis. The IP2 lifetime was around 2 h, longer than that (half an hour) of IP1, which may be associated with the rapid cooling and stronger inversion in the lower level below the melting layer. Eventually, IP appears to occur in the thermodynamic condition of both cold air intrusion in the lower atmosphere and an existing warmer layer aloft.

We examined general characteristics of ice pellets, quantitatively measured for the first time in Korea, and investigated the meteorological condition in association with IP occurrence. However, IP particles captured in the camera were very few (only 60) because of short lifetime (within a couple of hours), and thus microphysical analysis of IP was very limited. Therefore, this study lacks a detailed microphysical analysis of ice pellet particles such as ice pellet types (bulged, spherical, fractured etc.) and ice particle surface including crack and fracture in associated with drag coefficient, as shown in Nagumo and Fujiyoshi (2015). Certainly, the next study should be focused on microphysical interpretation of ice pellet particles in the favorable conditions for IP occurrence.

We also need more intensive observations to explore IP episodes and further to understand the various roles of frequent-occurring cold air intrusion with barrier wind in wintertime solid precipitation. Since freezing precipitation (FP) is a short-lived and mesoscale phenomenon during the phase change of solid precipitation, it is difficult to appropriately capture its occurrence. Therefore, in case of snowfall, we need to continuously measure snow characteristics with a MASC together with remote sensing and atmospheric thermodynamics (radar, wind profiler, rawinsonde etc.) to understand its microphysics and long-term climatology. This kind of study on the phase change of solid precipitation would contribute to preventing severe traffic accident as well as aircraft icing problem.

Acknowledgements This work was supported by the National Research Foundation of grant funded by the Korean government (NRF-2022R1F1A1063196), and also partly supported by Forecast Research Department and Research Application Department of National Institute of Meteorological Sciences (NIMS). We also appreciate the reviewers for the valuable and constructive comments which significantly improved the original version.

Open Access This article is licensed under a Creative Commons Attribution 4.0 International License, which permits use, sharing, adaptation, distribution and reproduction in any medium or format, as long as you give appropriate credit to the original author(s) and the source, provide a link to the Creative Commons licence, and indicate if changes were made. The images or other third party material in this article are included in the article's Creative Commons licence, unless indicated

otherwise in a credit line to the material. If material is not included in the article's Creative Commons licence and your intended use is not permitted by statutory regulation or exceeds the permitted use, you will need to obtain permission directly from the copyright holder. To view a copy of this licence, visit <http://creativecommons.org/licenses/by/4.0/>.

References

- Atlas, D., Ulbrich, C.W.: Path-and area-integrated rainfall measurement by microwave attenuation in the 1–3 cm band. *J. Appl. Meteor.* **16**(12), 1322–1331 (1977). [https://doi.org/10.1175/1520-0450\(1977\)016%3c1322:PAAIRM%3e2.0.CO;2](https://doi.org/10.1175/1520-0450(1977)016%3c1322:PAAIRM%3e2.0.CO;2)
- Bernstein, B.C.: Regional and local influences on freezing drizzle, freezing rain, and ice pellet events. *Weather Forecast.* **15**(5), 485–508 (2000). [https://doi.org/10.1175/1520-0434\(2000\)015%3c0485:RALIOF%3e2.0.CO;2](https://doi.org/10.1175/1520-0434(2000)015%3c0485:RALIOF%3e2.0.CO;2)
- Bernstein, B.C., Omeron, T.A.: Coauthors: Surface weather features associated with freezing precipitation and severe in-flight aircraft icing. *Atmos. Res.* **46**, 57–73 (1998). [https://doi.org/10.1016/S0169-8095\(97\)00051-3](https://doi.org/10.1016/S0169-8095(97)00051-3)
- Bourgouin, P.: A method to determine precipitation types. *Weather Forecast.* **15**(5), 583–592 (2000). [https://doi.org/10.1175/1520-0434\(2000\)015%3c0583:AMTDP%3e2.0.CO;2](https://doi.org/10.1175/1520-0434(2000)015%3c0583:AMTDP%3e2.0.CO;2)
- Carmichael, H., Stewart, R.E., Henson, W., Theriault, J.: Environmental conditions favoring ice pellet aggregation. *Atmos. Res.* **101**, 844–851 (2011). <https://doi.org/10.1016/j.atmosres.2011.05.015>
- Cortinas, J.V., Bernstein, B.C., Jr., Robbins, C.C., Strapp, J.W.: An analysis of freezing rain, freezing drizzle, and ice pellets across the United States and Canada: 1976–90. *Weather Forecast.* **19**, 377–390 (2004). [https://doi.org/10.1175/1520-0434\(2004\)019%3c0377:AAOFRF%3e2.0.CO;2](https://doi.org/10.1175/1520-0434(2004)019%3c0377:AAOFRF%3e2.0.CO;2)
- Deng, D., Gao, S., Hu, L., Du, X., Wang, J., Wang, C.: The impact of Guizhou topography on the distribution of freezing rain in early January 2011. *Q. J. R. Meteorol. Soc.* **141**, 3252–3326 (2015). <https://doi.org/10.1002/qj.2607>
- Gao, Y., Wu, T., Chen, B., Wang, J., Liu, Y.: A numerical simulation of microphysical structure of cloud associated with the 2008 winter freezing rain over Southern China. *J. Meteor. Soc. Jpn.* **91**, 101–117 (2013). <https://doi.org/10.2151/jmsj.2013-202>
- Garrett, T.J., Fallgatter, C., Shkurko, K., Howlett, D.: Fall speed measurement and high-resolution multi-angle photography of hydrometeors in free fall. *Atmos. Meas. Tech.* **5**(11), 2625–2633 (2012). <https://doi.org/10.5194/amt-5-2625-2012>
- Gibson, S.R., Stewart, R.E.: Observations of ice pellets during a winter storm. *Atmos. Res.* **85**(1), 64–76 (2007). <https://doi.org/10.1016/j.atmosres.2006.11.004>
- Hanesiak, J.M., Stewart, R.E.: The mesoscale and microscale structure of a severe ice pellet storm. *Mon. Weather Rev.* **123**(11), 3144–3162 (1995). [https://doi.org/10.1175/1520-0493\(1995\)123%3c3144:TMAMSO%3e2.0.CO;2](https://doi.org/10.1175/1520-0493(1995)123%3c3144:TMAMSO%3e2.0.CO;2)
- Houston, T.G., Changnon, S.A.: Freezing rain events: a major weather hazard in the conterminous United States. *Nat. Hazards* **40**, 485–494 (2007). <https://doi.org/10.1007/s11069-006-9006-0>
- Ishizaka, M.: Measurement of falling velocity of rimed snowflakes. *J. Jpn. Assoc. Snow Ice* **57**(3), 229–238 (1995). <https://doi.org/10.5331/seppyo.57.229>
- Ishizaka, M., Motoyoshi, H., Nakai, S., Shiina, T., Kumakura, T., Muramoto, K.I.: A new method for identifying the main type of solid hydrometeors contributing to snowfall from measured size-fall speed relationship. *J. Meteor. Soc. Jpn.* **91**(6), 747–762 (2013). <https://doi.org/10.2151/jmsj.2013-602>

- Kim, Y.-J., Kim, B.-G., Shim, J.-K., Choi, B.-C.: Observation and numerical simulation of cold clouds and snow particles in the Yeongdong Region. *Asia-Pac. J. Atmos. Sci.* **54**(3), 499–510 (2018). <https://doi.org/10.1007/s13143-018-0055-6>
- Kim, B.-G., Kim, M.-G., Kwon, T.-Y.: Coauthors: observation and understanding of snowfall characteristics in the Yeongdong region. *Atmosphere* **31**(4), 461–472 (2021a). <https://doi.org/10.14191/Atmos.2021.31.4.461>. (in Korean with English abstract)
- Kim, M.-G., Kim, B.-G., Eun, S.-H., Chae, Y.-J., Jeong, J.-H., Choi, Y.-G., Park, G.-M.: Analysis of the relationship of cold air damping with snowfall in the Yeongdong region. *Atmosphere* **31**(4), 421–431 (2021b). <https://doi.org/10.14191/Atmos.2021.31.4.421>. (in Korean with English abstract)
- Ko, A.R., Kim, B.-G., Eun, S.H., Park, Y.S., Choi, B.C.: Analysis of the relationship of water vapor with precipitation for the winter ESSAY period. *Atmosphere* **26**(1), 19–33 (2016). <https://doi.org/10.14191/Atmos.2016.26.1.019>. (in Korean with English abstract)
- Kochtubajda, B., Mooney, C., Stewart, R.: Characteristics, atmospheric drivers and occurrence patterns of freezing precipitation and ice pellets over the Prairie Provinces and Arctic Territories of Canada: 1964–2005. *Atmos. Res.* **191**, 115–127 (2017). <https://doi.org/10.1016/j.atmosres.2017.03.005>
- Lee, J.-H., Eun, S.-H., Kim, B.-G., Han, S.-O.: An analysis of low-level stability in the heavy snowfall event observed in the Yeongdong Region. *Atmosphere* **22**(2), 209–219 (2012). <https://doi.org/10.14191/Atmos.2012.22.2.209>. (in Korean with English abstract)
- Matsushita, H., Nishio, F.: A simple method of discriminating between occurrences of freezing rain and ice pellets in the Kanto Plain, Japan. *J. Meteor. Soc. Jpn.* **86**, 633–648 (2008). <https://doi.org/10.2151/jmsj.86.633>
- Nagumo, N., Fujiyoshi, Y.: Microphysical properties of slow-falling and fast-falling ice pellets formed by freezing associated with evaporative cooling. *Mon. Weather Rev.* **143**, 4376–4392 (2015). <https://doi.org/10.1175/MWR-D-15-0054.1>
- Nagumo, N., Fujiyoshi, Y.: Synoptic-scale environmental features of the long-lasting ice pellet event in Northern Japan on 10 April 2005. *Mon. Weather Rev.* **145**, 899–907 (2017). <https://doi.org/10.1175/MWR-D-16-0361.1>
- Nam, H.-G., Kim, B.-G., Han, S.-O.: Coauthors: Characteristics of easterly-induced snowfall in Yeongdong and its relationship to air-sea temperature difference. *Asia-Pac. J. Atmos. Sci.* **50**(4), 541–552 (2014). <https://doi.org/10.1007/s13143-014-0044-3>
- Praz, C., Roulet, Y.-A., Berne, A.: Solid hydrometeor classification and riming degree estimation from pictures collected with a Multi-Angle Snowflake Camera. *Atmos. Meas. Tech.* **10**, 1335–1357 (2017). <https://doi.org/10.5194/amt-10-1335-2017>
- Ralph, M.F., Coauthors: Improving short term (0–48 h) cool-season quantitative precipitation forecasting: recommendations from a USWRP workshop. *Bull. Amer. Meteor. Soc.* **86**, 1619–1632 (2005). <https://doi.org/10.1175/BAMS-86-11-1619>
- Rauber, R.M., Coauthors: The relative importance of warm rain and melting processes in freezing precipitation events. *J. App. Meteor.* **39**(7), 1185–1195 (2000). [https://doi.org/10.1175/1520-0450\(2000\)039%3c1185:TRIOWR%3e2.0.CO;2](https://doi.org/10.1175/1520-0450(2000)039%3c1185:TRIOWR%3e2.0.CO;2)
- Rauber, R.M., Olthoff, L.S., Ramamurthy, M.K., Miller, D., Kunkel, K.E.: A synoptic weather pattern and sounding-based climatology of freezing precipitation in the United States East of the rocky mountains. *J. App. Meteor.* **40**(10), 1724–1747 (2001). [https://doi.org/10.1175/1520-0450\(2001\)040%3c1724:ASWPAS%3e2.0.CO;2](https://doi.org/10.1175/1520-0450(2001)040%3c1724:ASWPAS%3e2.0.CO;2)
- Roberts, E., Stewart, R.E.: On the occurrence of freezing rain and ice pellets over the eastern Canadian Arctic. *Atmos. Res.* **89**(1), 93–109 (2008). <https://doi.org/10.1016/j.atmosres.2007.11.032>
- Schuur, T.J., Park, H.-S., Ryzhkov, A.V., Reeves, H.D.: Classification of precipitation types during transitional winter weather using the RUC model and polarimetric radar retrievals. *J. App. Meteor.* **51**(4), 763–779 (2012). <https://doi.org/10.1175/JAMC-D-11-091.1>
- Shin, H.C., Ha, J.H., Ahn, K.D., Lee, E.H., Kim, C.H., Lee, Y.H., Clayton, A.: An overview of KMA's operational NWP data assimilation systems. *Data Assimilation Atmos. Ocean. Hydrol. Appl.* **IV**, 665–687 (2022)
- Stewart, R.E., Crawford, R.W.: Some characteristics of the precipitation formed within winter storms over eastern Newfoundland. *Atmos. Res.* **36**, 17–37 (1995). [https://doi.org/10.1016/0169-8095\(94\)00004-W](https://doi.org/10.1016/0169-8095(94)00004-W)

Publisher's Note Springer Nature remains neutral with regard to jurisdictional claims in published maps and institutional affiliations.

